PREPARED FOR THE U.S. DEPARTMENT OF ENERGY,
UNDER CONTRACT DE-AC02-76CH03073

PPPL-3751
UC-70

PPPL-3751

Global Extended MHD Studies of Fast Magnetic Reconnection

by

J.A. Breslau and S.C. Jardin

September 2002

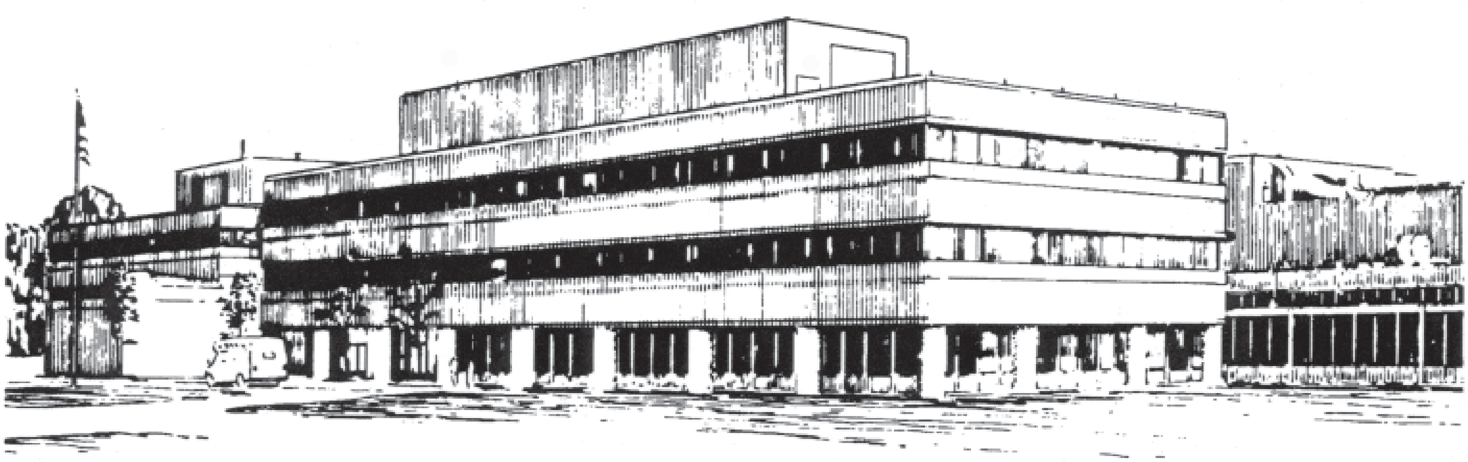

PRINCETON PLASMA PHYSICS LABORATORY
PRINCETON UNIVERSITY, PRINCETON, NEW JERSEY

PPPL Reports Disclaimer

This report was prepared as an account of work sponsored by an agency of the United States Government. Neither the United States Government nor any agency thereof, nor any of their employees, makes any warranty, express or implied, or assumes any legal liability or responsibility for the accuracy, completeness, or usefulness of any information, apparatus, product, or process disclosed, or represents that its use would not infringe privately owned rights. Reference herein to any specific commercial product, process, or service by trade name, trademark, manufacturer, or otherwise, does not necessarily constitute or imply its endorsement, recommendation, or favoring by the United States Government or any agency thereof. The views and opinions of authors expressed herein do not necessarily state or reflect those of the United States Government or any agency thereof.

Availability

This report is posted on the U.S. Department of Energy's Princeton Plasma Physics Laboratory Publications and Reports web site in Fiscal Year 2002. The home page for PPPL Reports and Publications is: http://www.pppl.gov/pub_report/

DOE and DOE Contractors can obtain copies of this report from:

U.S. Department of Energy
Office of Scientific and Technical Information
DOE Technical Information Services (DTIS)
P.O. Box 62
Oak Ridge, TN 37831

Telephone: (865) 576-8401

Fax: (865) 576-5728

Email: reports@adonis.osti.gov

This report is available to the general public from:

National Technical Information Service
U.S. Department of Commerce
5285 Port Royal Road
Springfield, VA 22161

Telephone: 1-800-553-6847 or
(703) 605-6000

Fax: (703) 321-8547

Internet: http://www.ntis.gov/ordering.htm

Global Extended MHD Studies of Fast Magnetic Reconnection

J. A. Breslau and S. C. Jardin
Princeton Plasma Physics Laboratory, P.O. Box 451, Princeton, New Jersey 08543

Abstract
Recent experimental and theoretical results have led to two lines of thought regarding the physical processes underlying fast magnetic reconnection. One is based on the traditional Sweet-Parker model but replaces the Spitzer resistivity with an enhanced resistivity caused by electron scattering by ion acoustic turbulence. The other includes the finite gyroradius effects that enter Ohm's law through the Hall and electron pressure gradient terms. A 2D numerical study, conducted with a new implicit parallel two-fluid code, has helped to clarify the similarities and differences in predictions between these two models and provides some insight into their respective ranges of validity.

1 Introduction

It is now generally accepted that two-dimensional magnetic reconnection can occur at rates that substantially exceed those predicted by the classical theory of Sweet and Parker.[1] Significant progress has been made in recent years in advancing the theoretical understanding of this fast magnetic reconnection. Contributions have come both from dedicated experiments such as the TS-3 device[2] and the Magnetic Reconnection Experiment (MRX);[3] and from many numerical studies carried out to test theoretical concepts.

There remain, however, two competing paradigms for explaining fast reconnection. One invokes enhanced "anomalous" resistivity and the geometrical effects that follow from it. This picture aims to explain the accelerated reconnection within the bounds of resistive MHD.[4,5] It is a collisional model in which a mechanism is invoked to elevate the resistivity in the reconnection current sheet to several times the Spitzer value. Because the magnitude of the resistivity and its gradient in this region determine the rate of reconnection in the MHD description, one can match any observed reconnection rate given a sufficiently large local resistivity.

The challenge of explaining fast reconnection in extremely high Lundquist number regimes such as the solar corona has led to an alternate, collisionless model. Critical to this model are finite gyroradius and electron inertia effects beyond the scope of MHD (but generally capable of being incorporated into so-called "extended MHD" fluid models). These new terms in the equations result in the creation of an inner region within the current sheet where the ions are unmagnetized and the governing electron MHD equations bring whistler physics into play. This can result in rapid reconnection flow rates that are essentially independent of the resistivity.[6]

The collisionless model's severe scale separation poses a considerable challenge to the numerical modeler, even beyond the usual one encountered in reconnection studies. Two numerical approaches are in common use for addressing the separation of scales in the standard reconnection problem between the outer quasi-ideal region and the inner diffusive region. One approach[7] is to restrict attention to the diffusion region only. This has the advantage of allowing very efficient solutions, but the disadvantage of requiring the specification of boundary conditions for the plasma inflow and outflow rates. The second approach[8] is to model the global plasma using the equations of reduced MHD, which contain a greatly reduced number of time advancement variables and timescales. This avoids the boundary condition difficulty but omits a number of potentially important physical effects.

The approach described here is to address the reconnection problem with a new implicit parallel algorithm that is efficient enough to allow solution of the global problem while advancing the full set of extended MHD equations with enough detail to fully resolve the inner region.[9] In Section 2 below, we describe the nature of the algorithm and the conditions of our simulations. Section 3 briefly describes an application of this method to reconnection in the relatively well-understood MHD regime. In Sections 4 and 5, we set forth some new results relating to "anomalous" resistivity and Hall reconnection respectively and connect these with previous work.

2 Numerical Method

We use the 2D Magnetic Reconnection Code (MRC) in this work.[9] It is based on a parallel implicit algorithm that time-advances either the two-fluid extended MHD equations or their single-fluid resistive MHD subset on a fixed, non-uniform, two-dimensional rectangular mesh. The geometry may be either cylindrical, with mesh coordinates R and z (and angle ϕ considered ignorable) to model spheromak or tokamak-like configurations; or Cartesian, using coordinates x and z, with y ignorable. Typical mesh dimensions are approximately 100 zones in the $\hat{x}$ direction, and between 500 and 1000 in $\hat{z}$, with z spacing in the current sheet region approximately one-fourth that of the quasi-ideal region. Fig. 1 illustrates the kind of resolution that can be achieved with these values.

2.1 Equations

The complete set of normalized equations advanced by MRC includes:

continuity:

$$\frac{\partial \rho}{\partial t} + \nabla \cdot (\rho \mathbf{v}) = 0 \tag{1}$$

force balance:

$$\rho \left(\frac{\partial \mathbf{v}}{\partial t} + \mathbf{v} \cdot \nabla \mathbf{v} \right) = \mathbf{J} \times \mathbf{B} - \nabla p + \nu \nabla^2 \mathbf{v} + \mathbf{M}_H \tag{2}$$

low-frequency Maxwell's equations:

$$\frac{\partial \mathbf{B}}{\partial t} = -\nabla \times \mathbf{E} \tag{3a}$$

$$\mathbf{J} = \nabla \times \mathbf{B} \tag{3b}$$

$$\nabla \cdot \mathbf{B} = 0 \tag{3c}$$

generalized Ohm's law:

$$\mathbf{E} \; + \; \mathbf{v} \times \mathbf{B} = \eta \mathbf{J} + \frac{\mathbf{J} \times \mathbf{B} - \nabla p_e}{ne} + \mathbf{R}_H \tag{4}$$

electron and ion pressure equations:

$$\frac{\partial p_e}{\partial t} + \mathbf{v}_e \cdot \nabla p_e = -\frac{5}{3} p_e \nabla \cdot \mathbf{v}_e + \frac{2}{3} \left[\eta |\mathbf{J}|^2 + \nabla \cdot \left(m_i \kappa_e \nabla \frac{p_e}{\rho} \right) - Q \right] \tag{5}$$

$$\frac{\partial p_i}{\partial t} + \mathbf{v} \cdot \nabla p_i = -\frac{5}{3} p_i \nabla \cdot \mathbf{v} + \frac{2}{3} \left[\nu ||\nabla \mathbf{v}||^2 + \nabla \cdot \left(m_i \kappa_i \nabla \frac{p_i}{\rho} \right) + Q \right]. \tag{6}$$

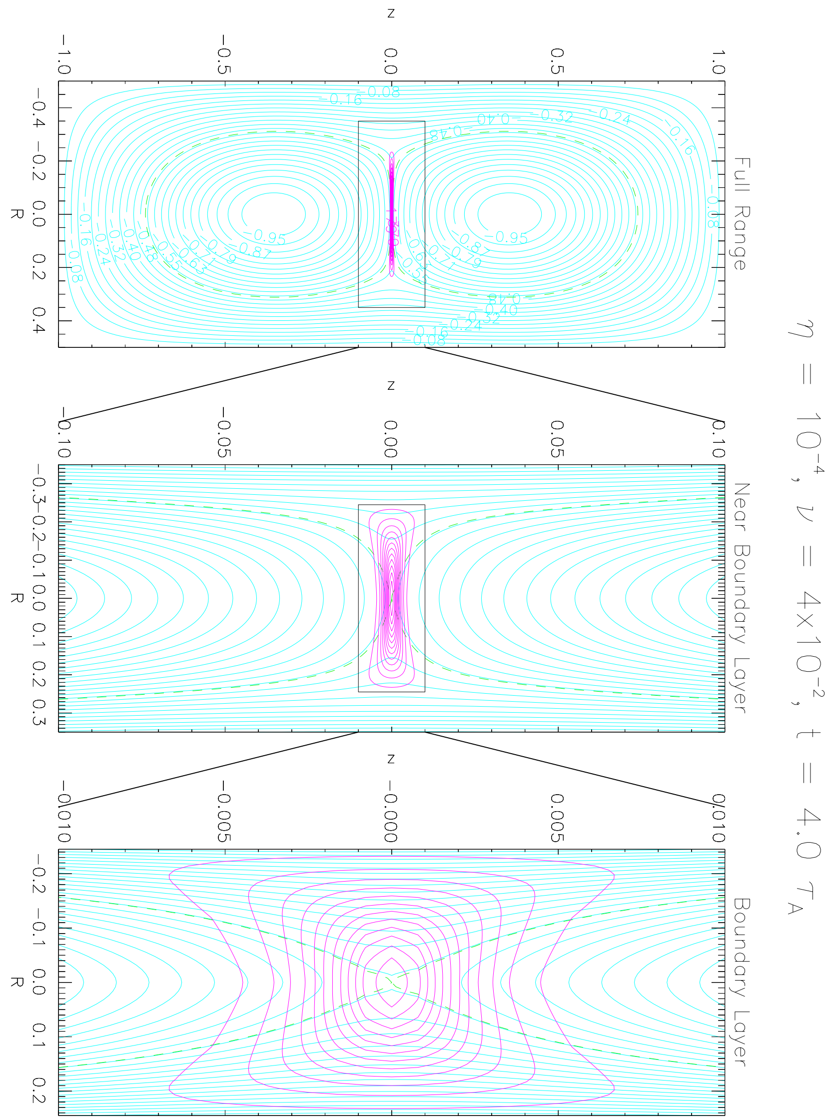

Figure 1: Resolution of global region and boundary layer in co-helicity MHD reconnection, Cartesian geometry: poloidal flux and toroidal current density contours. Successive plots are magnified 10× in the z direction. The dashed line is the separatrix.

Here ρ is the mass density, $\mathbf{v}_e = \mathbf{v} - \mathbf{J}/ne$ is the electron fluid velocity, $p = p_e + p_i$ is the sum of the electron and ion fluid pressures, ν is the viscosity, η is the resistivity, $\kappa_{e,i}$ are the thermal conductivities, and Q represents the transfer of heat between the two species as specified by Braginskii.[10] With the exception of the "anomalous resistivity" cases discussed in Section 4, the transport coefficients are isotropic and constant in time and space.

The terms $\mathbf{M}_H \propto -\nabla^4\mathbf{v}$ and $\mathbf{R}_H \propto -\nabla^2\mathbf{J}$ are fourth-order dissipative terms added to the momentum and Ohm's law equations to provide small artificial hyper-viscosity and hyper-resistivity that prove necessary to damp out grid-scale oscillations associated with the whistler mode introduced by the Hall term. Scaling studies have been conducted[9] on these terms to ensure that their inclusion does not significantly alter the physics of the problem, except as noted below.

2.2 Initial and boundary conditions

MRC has been constructed to model, in a somewhat idealized way, laboratory experiments such as TS-3[2] and MRX[3] that were designed to investigate magnetic reconnection in the context of merging spheromaks. Its initial conditions consist of a pair of spheromaks (in the cylindrical geometry case) or straight flux cylinders (in the Cartesian case) with parallel out-of-plane currents that tend to draw them together. The merging is classified as "co-helicity", "counter-helicity", or "null helicity" according to the relative orientations of the out-of-plane magnetic fields of the flux tubes: parallel, anti-parallel, or identically zero, respectively. A third flux tube with oppositely directed out-of-plane current is initially inserted between the two that are to reconnect in order to provide an initial equilibrium. An analytic description of this three-island equilibrium determines the initial state of the plasma.

In the co-helicity case, a force-free Taylor state[11] that satisfies the equilibrium requirement in the absence of pressure gradients is employed. (In this case, the out-of-plane field plays the role of a pressure during the reconnection process.) In the other two cases, the in-plane fields and out-of-plane currents are identical to those of the co-helicity case. In the case of null helicity, there is no out-of-plane field, so the equilibrium condition in Cartesian geometry becomes

$$\nabla p = -\nabla^2\psi\nabla\psi \tag{7}$$

(where ψ is the poloidal flux function, which is kept zero on the computational boundary), which can be satisfied by setting $p(\psi) = p_0 + \lambda^2\psi^2/2$, along with

$$\nabla^2\psi = -\lambda^2\psi. \tag{8}$$

In the counter-helicity case, equal and opposite out-of-plane fluxes satisfying the Taylor state are used for the upper and lower islands, while the central island has no flux and uses the above pressure formulation instead.

To initiate merging, the central island is destroyed rapidly by applying an artificially elevated resistivity to the region it occupies. (This resistivity is dependent on the sign of ψ, which is positive for the central island and negative for the other two. The resistivity is high and constant in the $\psi > 0$ region, and low and constant in the $\psi < 0$ region, with a smooth transition for $0 < \psi \ll 1$ in between.) Once the central island has vanished, which takes less than a single Alfvén time, the other two islands begin to coalesce under conditions of constant resistivity. This initial phase is illustrated in the first two frames of Figs. 7 and 8.

Conducting wall boundary conditions are used in this work. These are implemented by applying $\mathbf{E} \times \hat{n} = 0$ and $\mathbf{v} \cdot \hat{n} = 0$ at the boundary, where $\hat{n}$ is the local normal. In addition, we find that numerical stability for the two-fluid cases is improved by the use of an elevated viscosity in the vicinity of the walls. This viscosity has a typical normalized value of 0.1 and falls off exponentially with distance from the walls with a scale length of about 5% of the system size, making it wholly negligible in the diffusion region.

3 Resistive MHD Reconnection

The resistive MHD equations are the subset of (1)–(6) formed by dropping the term proportional to $1/ne$ from (4) and summing (5) and (6) to get a single equation for the pressure. The behavior of a reconnecting plasma obeying the equations of resistive MHD is well established.[1] The reconnection, if unforced, occurs on a timescale that is asymptotically the geometric mean of the resistive and advective timescales, i.e., at a rate proportional to $S^{-1/2}$, where S is the Lundquist number,

$$S = \frac{\tau_R}{\tau_A} = \frac{L v_A}{\eta}, \tag{9}$$

L being the characteristic scale length of field gradients, and v_A the Alfvén speed. This initial baseline study consists of a scan over resistivity from 10^{-5} to 10^{-3} and over viscosity from 10^{-4} to 10^{-1} to study resistive MHD reconnection in Cartesian geometry for all three relative helicities. The key quantity to be tracked is the total reconnection time t_{rec}, defined here as the time elapsed between the formation of the X-point within the current sheet when the central island has vanished; and its disappearance as the other two islands complete their merging.

3.1 Laminar Results

The results of this baseline resistive MHD study are shown in Figs. 2, 3, and 4 and are summarized in Table 1. For co-helicity merging (Fig. 2), the reconnection time scales with the

Table 1: Reconnection rates shown in Figs. 2–4 scale as $\eta^{-x}\nu^{y}$.

Helicity	x	y
co-helicity	0.6	0.3
counter-helicity	0.40 – 0.48	0.26 – 0.34
null helicity	0.3	0.23 – 0.26

resistivity as $t_{rec} \propto \eta^{-0.60}$ and with the viscosity as $t_{rec} \propto \nu^{0.3}$. The three fits shown in Fig. 3 for the null helicity reconnection show that the reconnection time scales as $t_{rec} \propto \eta^{-0.3}$. This implies that at small values of the resistivity, the null helicity reconnection time can be considerably faster than that for the corresponding co-helicity case. The scaling for the reconnection time for the counter-helicity configuration, as shown in Fig. 4, is intermediate between those of the corresponding co- and null helicity rates shown in Figs. 2 and 3.

The expected MHD scaling of reconnection rates, including the effects of viscosity, is[12]

$$\dot{\psi} \propto \eta^{1/2} \left(1 + \nu/\eta\right)^{-1/4} \tag{10}$$

for a Sweet-Parker-type (elongated) reconnection layer. Given that ν and η are of the same order in our study, putting it in between the two asymptotic regimes defined by (10); and that our model is fully compressible, unlike Sweet-Parker, our results show reasonably good agreement with this prediction.

3.2 Tearing Instability

In addition to reconnection rates, current sheet geometries show strong agreement with Sweet-Parker predictions: the sheet thickness δ in the inflow direction is proportional to $\eta^{1/2}$, while its width L in the outflow direction remains macroscopic, and is determined by

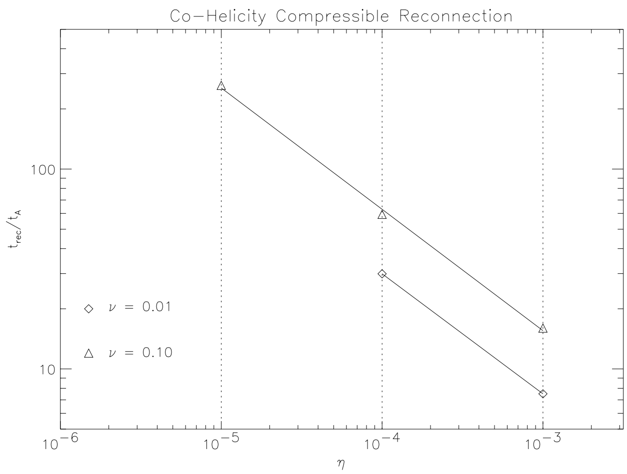

Figure 2: Scaling of co-helicity compressible reconnection time with resistivity and viscosity. Cartesian geometry.

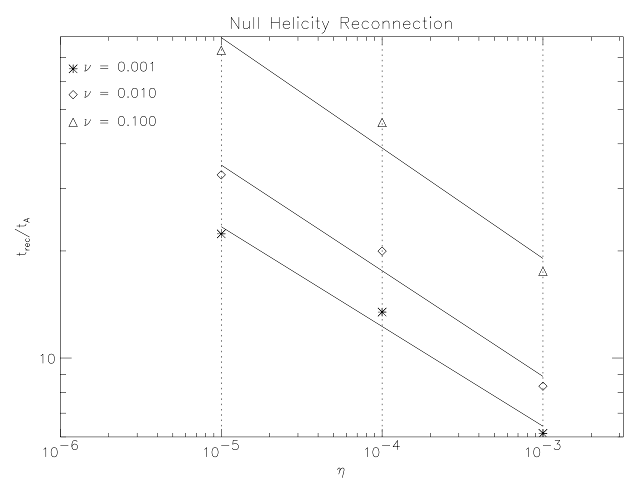

Figure 3: Scaling of null helicity reconnection time with resistivity and viscosity. Cartesian geometry.

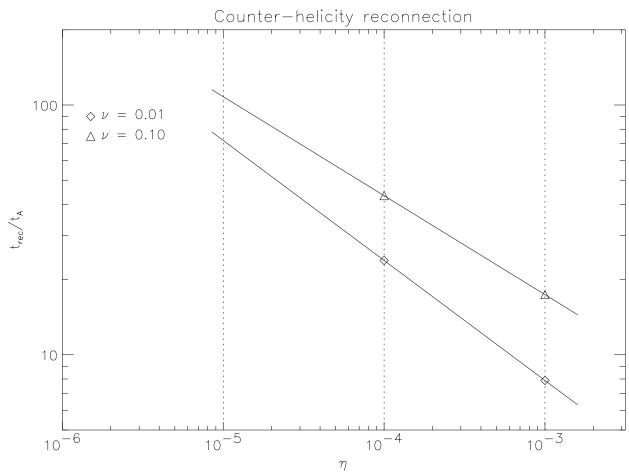

Figure 4: Scaling of counter-helicity reconnection time with resistivity and viscosity. Cartesian geometry.

the scale length of the field gradient (Fig. 1). For sufficiently small aspect ratio δ/L in the null helicity and co-helicity cases, the current sheet is broken up by a tearing instability. The X-point divides into a pair of X-points separated by an O-point (Fig. 5). The island around the O-point quickly saturates, backing up the reconnection inflow, and causing the rate to drop to the resistive time scale. The assumed symmetry of the problem domain prevents the island from being swept outward (which would result in “patchy” reconnection[14]). The critical value of η necessary for the onset of the instability is consistent with the quasi-empirical criterion

$$L/\delta > 7 \coth\left(\frac{8}{S^{1/2}}\right) \tag{11}$$

set forth by Lee and Fu in 1986.[15]

4 Anomalous Resistivity Study

4.1 Motivation

The experimentally observed values of the reconnection rate are significantly larger than those predicted in Table 1. Since the reconnection rate has been shown to be proportional to the resistivity to some power, it has been postulated that the fast reconnection is simply due to an anomalously large value of the effective resistivity.

Evidence of enhanced resistivity is provided by recent results from the Magnetic Reconnection Experiment (MRX). Direct measurement of the ratio of electric to magnetic fields in that device yields an effective perpendicular resistivity that may exceed the Spitzer value by as much as a factor of ten.[4] Based on this effective resistivity, Ji and co-workers have found a good fit to the Sweet-Parker theory, suitably modified to include the effects of compressibility and downstream pressure.

The prevailing theoretical model of enhanced resistivity is one in which high electron drift velocity is limited by the onset of localized microinstabilities associated with ion acoustic turbulence.[16] The effect of these instabilities would be a local increase in the effective resistivity in proportion to the amount by which the drift speed exceeds the ion sound speed.

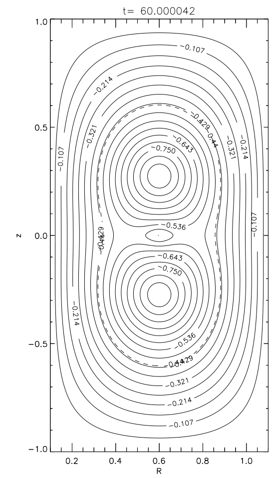

Figure 5: Poloidal flux contours during the stagnation phase of patchy null helicity MHD reconnection. $\eta = 10^{-5}, \nu = 10^{-4}$.

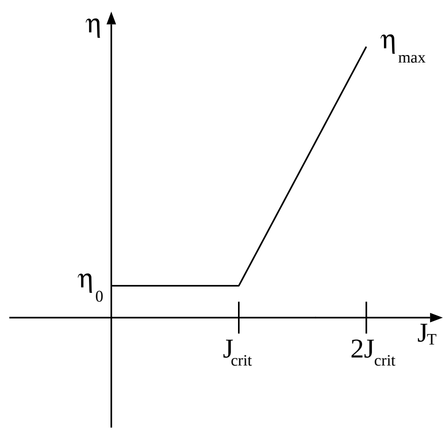

Figure 6: The resistivity model employed in the anomalous resistivity study.

Based on this theory, we construct a simplified model in which

$$\eta = \eta(J_T) = \begin{cases} \eta_0, & |J_T| \leq J_{crit} \\ \eta_0 + (\eta_{max} - \eta_0)\,\dfrac{(|J_T| - J_{crit})}{J_{crit}}, & |J_T| > J_{crit} \end{cases} \tag{12}$$

where J_T is the local toroidal current density, $\eta_0 \ll \eta_{max}$ is the "background" resistivity, J_{crit} is the current density at which the drift velocity is equal to the ion thermal speed, and $\eta_{max} = c^2/\omega_{pe}$ in appropriate units (see Fig. 6).

A simple two-dimensional analysis by Kulsrud[5] has shown that, whereas under the standard Sweet-Parker assumptions the predicted reconnection inflow rate for this model would be

$$v_{in}/v_{out} = \delta/L \propto J_{crit}^{-1} \tag{13}$$

(since $J_{crit} \propto B_0/\delta$ and L and B_0 are fixed), a more general, Petschek-like picture predicts something quite different.

Table 2: Data from the anomalous resistivity study. All quantities are evaluated at the peak reconnection rate.

J_{crit}	δ	L	v_{out}	δ/L	$(\delta/S_{eff}L)^{1/3}$	$\mathbf{v}_{in}/\mathbf{v}_{out}$
21.96	0.0575	0.16	0.856	0.36	0.58	**0.61**
43.92	0.0535	0.16	1.03	0.33	0.53	**0.40**
87.83	0.037	0.17	1.04	0.22	0.45	**0.33**
131.70	0.026	0.18	1.04	0.14	0.38	**0.34**
263.50	0.014	0.21	0.982	0.067	0.29	**0.27**
439.20	0.0075	0.235	0.846	0.032	0.23	**0.19**
527.00	0.006	0.235	0.778	0.026	0.22	**0.17**

In the original Petschek model,[17] the sheet width L' in the outflow direction may be much smaller than the system size L so that the sheet becomes microscopic while its aspect ratio δ/L' approaches unity. The reconnecting plasma is not, in this case, constrained to flow through the microscopic sheet but instead flows across standing shocks extending outward from its edges. The rate v_{in}/v_{out}, however, is still proportional to the aspect ratio.

Kulsrud's analysis begins with the Petschek supposition $L' \ll L$. The variation in the strength of the reconnecting field in the outflow direction is assumed to be quadratic about the X-point, while the resistivity varies linearly with the current density in this region. From the assumption of stationarity $\dot{\mathbf{B}} = 0$ it then follows that

$$\frac{\eta_{max}}{J_{crit}} \frac{v_{out}^2 L'}{\delta^2 L^2} \approx \frac{v_{out} v_{in}}{L'} \tag{14}$$

so that $L'/L \propto (J_{crit}/L)^{1/3}$ and

$$\frac{v_{in}}{v_{out}} \approx \left(\frac{\delta}{S_{eff} L}\right)^{1/3} \propto J_{crit}^{-1/3} \tag{15}$$

where $S_{eff} \equiv L v_A / \eta_{max}$. Thus in this model the presence of a resistivity gradient enhances the reconnection rate above the Sweet-Parker prediction by causing additional bending of the field lines, similar to what occurs in the Petschek theory.

4.2 Results

A series of simulations were run to distinguish between the two possibilities set forth above. All cases followed co-helicity reconnection with a fully compressible, single-fluid version of the code. The initial electron number density was held constant over the study at $n = 2 \times 10^{20}$ m^{-3} and the normalized pressure at $p = 0.5$, which together mandate a peak resistivity of $\eta_{max} = 0.0730$. The "background" resistivity for all cases was $\eta_0 = 10^{-4}$, while the viscosity was $\nu = 0.04$. The value of J_{crit} was varied systematically between 21.96 and 527.0. The results are summarized in Table 2.

The current sheet thickness δ was found to vary as J_{crit}^{-1} as expected. The thicker current sheet corresponds to a wider opening angle of the X-point, allowing plasma to pass through the diffusion region more rapidly. However, the reconnection rate, as characterized either by the ratio v_{in}/v_{out} during the quasi-steady reconnection phase, or the value of $\dot{\psi}$ at the X-point during this phase, is proportional to $J_{crit}^{-1/3}$, agreeing both qualitatively and quantitatively with the Kulsrud prediction. This study thus confirms the Kulsrud result that enhanced resistivity can substantially increase the reconnection rate, but the process is not

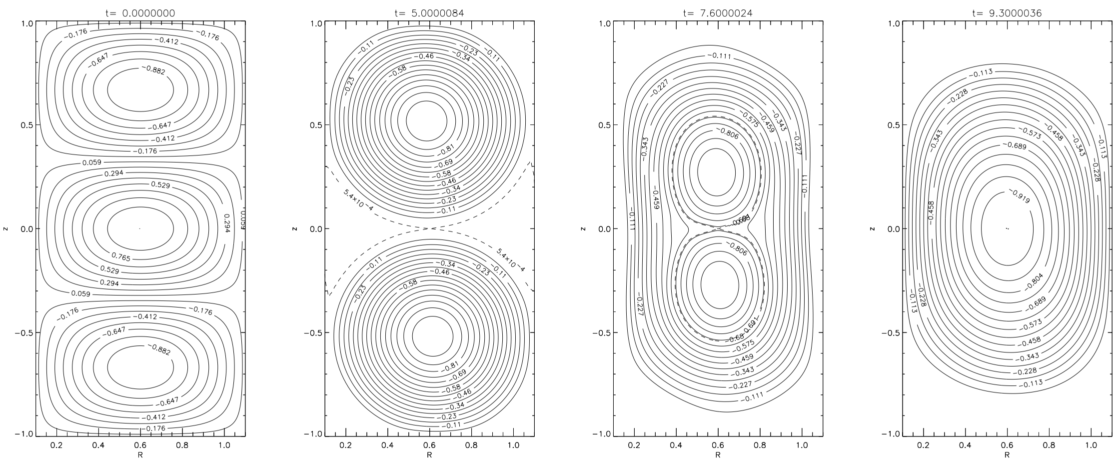

initial state middle island gone reconnecting decaying

Figure 7: Poloidal flux contours during successive phases of co-helicity Hall reconnection. Cartesian geometry, $\eta = 10^{-4}$, $\nu = 10^{-2}$, $\chi = 2.277 \times 10^{-2}$.

described by a mere enhancement of the effective resistivity within a simple Sweet-Parker model. However, it should be noted that these results cannot be taken as a confirmation of the original Petschek model, as the observed current sheets lack the two most conspicuous features of that model: they are macroscopic in the outflow direction (Fig. 12b) and are not associated with shocks of any kind.

5 Two-Fluid Effects

The two-fluid equations (1)–(6) can be expected to yield different results from those of resistive MHD if there is any region of the plasma in which the Hall and/or electron pressure gradient terms in Ohm's law become comparable in size to the other terms. In such a region, the field lines will become decoupled from the bulk plasma flow (which, because of the mass ratio, is essentially the ion flow) but will remain frozen into the electron fluid except in a much smaller region where dissipative or electron inertia effects become important. The strength of the Hall term, and thus the size of the region in which it dominates, is determined by the size of the $1/ne$ coefficient in front of it. When translated into the normalized units of the code, this becomes a dimensionless quantity (which we label "χ") equal to the ratio of the ion skin depth to the system size. To be consistent with the work described above, χ must take on a value of approximately 2.3×10^{-2}.

Co-helicity and null helicity two-fluid cases were run with initial conditions identical to those of the studies described above. The initial pressure distribution was partitioned such that $T_i = T_e$.

5.1 Co-helicity Results

With the inclusion of the Hall term, several qualitative changes are immediately evident, as shown in the flux contours in Fig. 7. One is a change in symmetry, leading to a tilt in the orientations of the islands with respect to one another. More signficantly, we see from comparing Figs. 1a and 7c that the region of contact between the merging islands is no longer an elongated flat current sheet as in the resistive MHD case, but instead has become

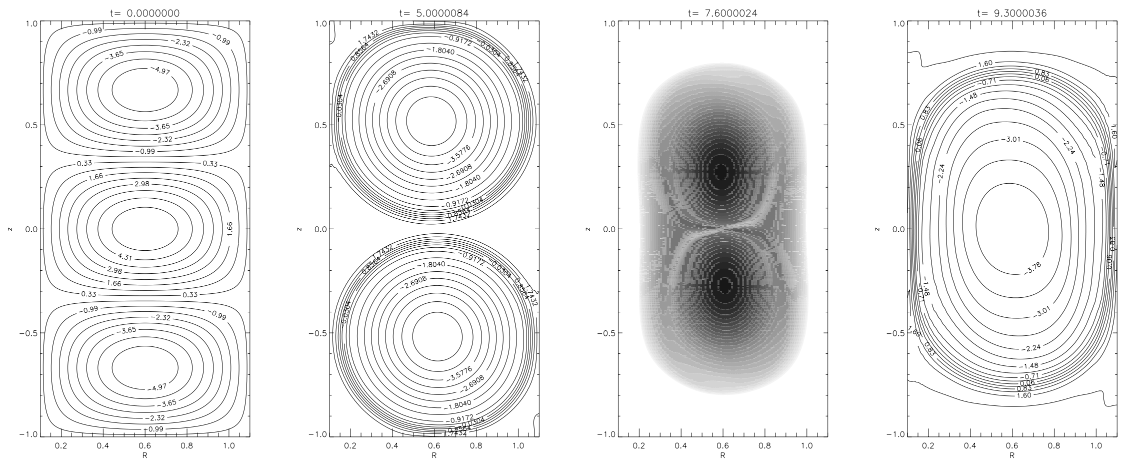

initial state | middle island gone | reconnecting | decaying

Figure 8: Toroidal field contours during successive phases of co-helicity Hall reconnection. Cartesian geometry, $\eta = 10^{-4}$, $\nu = 10^{-2}$, $\chi = 2.277 \times 10^{-2}$. The third figure is shown in grayscale to emphasize the quadrupole structure.

a single point of osculation. The current spike about this point has an aspect ratio of unity and a thickness intermediate between the Sweet-Parker and anomalous resistivity values. The out-of-plane magnetic field, as shown in Fig. 8, has a novel characteristic during the reconnection phase: it exhibits a quadrupolar perturbation about the X-point. The wide opening angle of the X-point leads to an outflow region substantially thicker than the current sheet itself (Fig. 10). The outflowing plasma in this region reaches a peak velocity twice that of the local Alfvén speed and shows significant viscous heating.

The starkest contrast between this and the resistive MHD cases can be seen in the out-of-plane electric field during the quasi-steady state phase of the reconnection. During this phase, $\dot{B}_z = -\partial_x E_y \approx 0$. The various contributions to E_y in the Ohm's law equation (4) are illustrated in Fig. 9 as a function of the coordinate x along the midplane $z = 0$. Whereas the resistive (ηJ_y) term necessarily plays the dominant role in the current sheet in Sweet-Parker reconnection, here it is everywhere negligible. The primary balance seen in the figure is between the convective ($\mathbf{v} \times \mathbf{B}$) term, dominant in the outflow region; and the Hall term, dominant about the X-point except at the very center, where dissipative effects are needed to break and reconnect the field lines and so the hyper-resistivity plays a small but fundamental role. (We surmise that electron inertia would take over this role were that term included in our treatment).

5.2 Null Helicity Results

The qualitative behavior of null helicity reconnection is similar to that of co-helicity reconnection. This similarity extends to the quadrupolar toroidal field, the magnitude of which is of the same order as that of the reconnecting poloidal field despite the fact that there is no initial toroidal field for these cases. This indicates that the decoupling of electrons and ions has the effect of strongly twisting the field into the out-of-plane direction. The outflow of the two fluids occurs on two different spatial scales, as shown in Fig. 10: the electrons flow out of the region much more rapidly (at approximately the whistler wave speed for a wavelength corresponding to the layer thickness) and in a narrower stream than the ions.

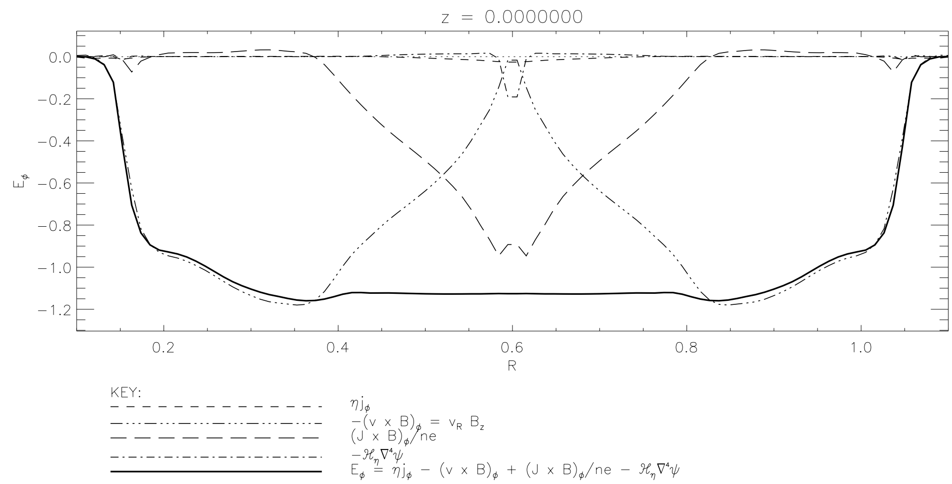

Figure 9: Out-of-plane electric field along the midplane during co-helicity Hall reconnection, by component. $\eta = 10^{-4}$, $\nu = 10^{-2}$, $\chi = 2.277 \times 10^{-2}$. Cartesian geometry.

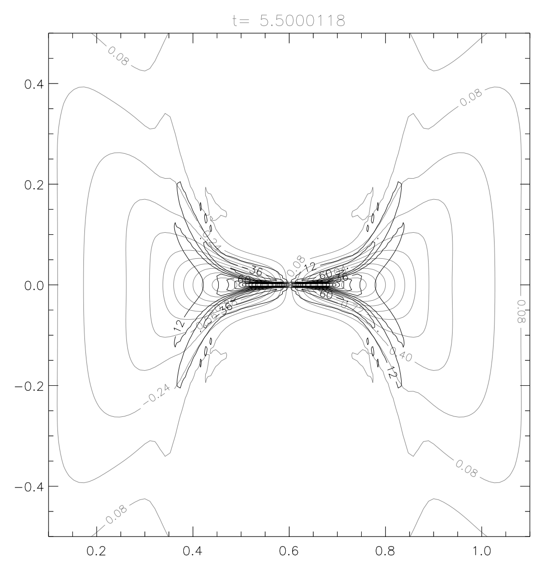

Figure 10: Contours of j_R (dark lines) and v_R during null helicity Hall reconnection. $\eta = 10^{-4}$, $\nu = 10^{-2}$, $\chi = 2.277 \times 10^{-2}$, $t = 5.5$. Peak $v_i = 1.6 v_A$; peak $v_e = v_i + 7.3 v_A$.

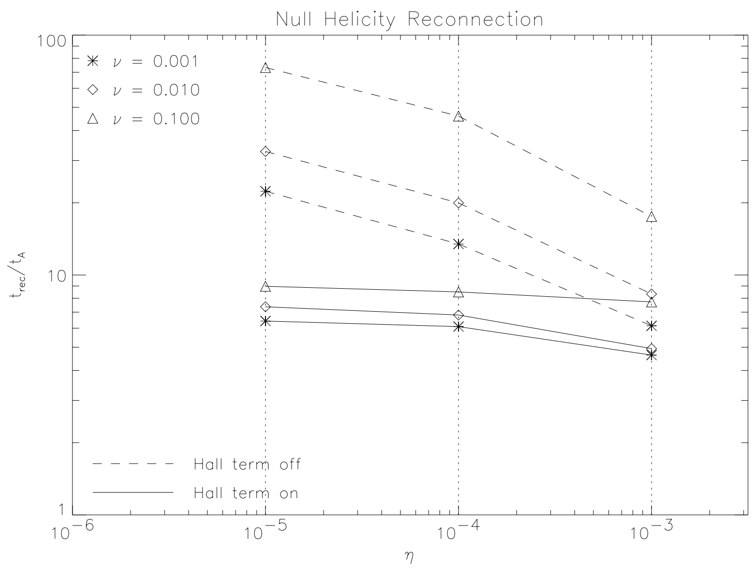

Figure 11: Comparison of MHD and two-fluid rate scalings of null helicity reconnection. Cartesian geometry.

The overall reconnection rate for both configurations is highly accelerated compared to that of resistive MHD. As indicated in Fig. 11, the dependence of the rate on the resistivity is also broken in the low-η limit, making this "fast reconnection" by definition. We also note that while the rate is highly sensitive to the value of the Hall parameter, it is quite insensitive to the size of the hyper-resistivity. So long as the diffusion region defined by the dissipative terms is smaller than an ion skin depth, the reconnection rate is determined by the Hall parameter. The current density in the diffusion region adjusts itself to the dominant dissipative parameter, in this case the hyper-resistivity, so as to keep the electric field constant in space.

5.3 Interpretation

The results in this section can be interpreted in terms of the two-fluid theory of collisionless reconnection.[18,6] In this theory, the region of the plasma sufficiently close to the X-point obeys the equations of electron MHD. The reconnecting field lines are thus frozen into the electron fluid, which is carrying the strong out-of-plane current. The sharp peaking of this current about the X-point indicates a strong shear in the out-of-plane electron velocity, resulting in a bending of the reconnecting in-plane field into the quadrupolar out-of-plane structure seen in Fig. 8c. In the steady state, this bending is balanced by convection of the out-of-plane field away from the X-point by electron flow in the outflow direction. The result of balancing these effects is that the out-of-plane field is of the same order as the reconnecting field; and the electron outflow occurs at the whistler speed based on the sheet thickness, while the inflow rate is independent of this thickness. Topological change (field line breaking) occurs within the much smaller region defined by the hyper-resistivity (or presumably, in a real collisionless plasma, by the electron inertial length); conventional resistivity does not come into play at all.

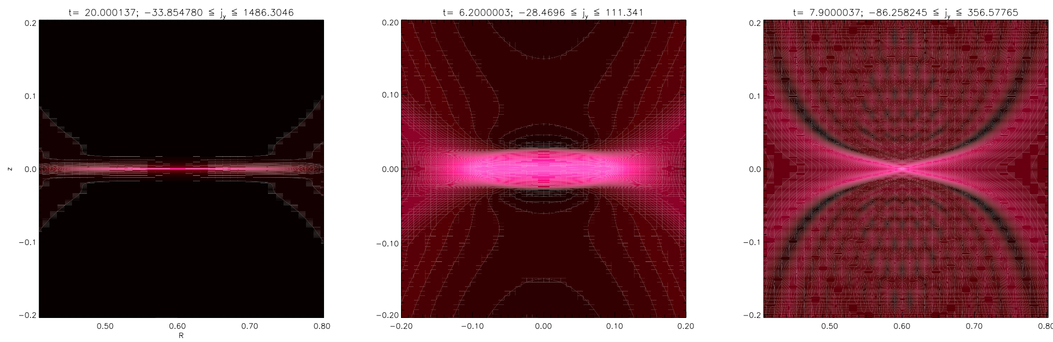

Figure 12: Typical out-of-plane current densities near the X-point during quasi-steady-state 2D reconnection. $\eta_0 = 10^{-4}$ for all cases. a. MHD. b. Anomalous resistivity, $J_{crit} = 132$. c. Two-fluid effects, $\chi = 2.3 \times 10^{-2}$.

6 Discussion

From the results of the foregoing sections, it is evident that either anomalous resistivity or the Hall term on its own is fully capable of giving rise to fast reconnection. In order to determine which (if either) of these two effects is playing the dominant role in a particular physical system, it is useful to compare the detailed predictions made by each study.

Anomalous resistivity accelerates reconnection in part by expanding the thickness δ of the current sheet (Fig. 12b). The Hall effect, in contrast, achieves a similar increase in aspect ratio by contracting the sheet width L (Fig. 12c). Anomalous resistivity is a collisional effect, and its dissipative nature is manifested in the coarse structure seen in the figure. The collisionless reconnection that takes place in the two-fluid case results in fine-scale structures, including a microscopic current sheet with X-shaped extensions, and a quadrupolar out-of-plane magnetic field. Diagnosing the out-of-plane field and measuring the shape of the current sheet in reconnection experiments are thus critical to resolving the question of which effect is predominant.

We note that while it is now clear that an enhanced resistivity can increase the reconnection rate substantially, the experimental justification of such a resistivity remains uncertain. Careful measurements of fluctuations in the MRX current sheet, for example, seem to indicate that the lower hybrid drift instability in that device, a priori the most promising candidate as a theoretical explanation of the enhancement, is not correlated with reconnection behavior and is unlikely to play a significant role in collisionless reconnection.[19] Additional non-turbulent physics should therefore be pursued.

7 Summary and Conclusions

We have presented simulation results obtained by solving the full set of extended MHD equations over a global domain but with enough resolution to fully resolve the inner reconnection region. These results support and extend conclusions reached based on previous local or reduced studies. Sweet-Parker reconnection is the correct result for two-dimensional constant-resistivity single-fluid MHD at moderate Lunquist numbers. At higher S, tearing instabilities set in and resistive MHD reconnection becomes slow or patchy. Standard resistive MHD is therefore inadequate for explaining fast reconnection.

In the presence of high, current-dependent resistivity within the MHD model, the X-point tends to open up and the Kulsrud scaling is observed. The resulting reconnection rate can be significantly higher than that predicted by the Sweet-Parker model, even taking the higher resistivity into account. Because the enhanced resistivity is postulated to depend on collisions, however, this model may have limited application in very high temperature plasmas.

Results were obtained for the global reconnecting plasma problem with the full two-fluid equations in the high Lundquist number regime. The results presented here bear out claims previously made about collisionless reconnection mechanisms based on reduced equation[20] or boundary layer[6] studies. Reconnection in this regime was shown to be rapid and independent of the plasma resistivity. The current sheet exhibits fine structures that differ qualitatively from those in the other two models. Simulations aimed at modeling bulk plasma phenomena on resistive time scales must include two-fluid effects to predict reconnection rates accurately.

Careful measurements will be required to adjudicate between the collisional and collisionless fast reconnection models in physical systems. Assessing the shape of the current sheet should provide the clearest indication of which effect predominates.

ACKNOWLEDGMENT

It is a pleasure to acknowledge useful discussions with T. Carter, J. Drake, H. Ji, R. Kulsrud, W. Park, and M. Yamada.

This work was supported by USDOE Contract No. DE-AC020-76-CH03073. One of us (JB) was supported by the Fusion Energy Sciences Fellowship Program, administered by the Oak Ridge Institute for Science and Education for the United States Department of Energy.

1. E. N. Parker, J. Geophys. Res. **62**, 509 (1957).
2. M. Yamada, F. W. Perkins, A. K. MacAulay, Y. Ono, and M. Katsurai, Phys. Fluids B **3**, 2379 (1991).
3. M. Yamada, H. Ji, T. Carter, S. Hsu, and Y. Ono, in *Proceedings of the 1996 International Conference on Plasma Physics* (Arakawa Printing Co., Ltd, Japan, 1996), Vol. 1, p. 558.
4. H. Ji, et. al., Phys. Rev. Lett. **80**, 3256 (1998).
5. R. Kulsrud, in *Proceedings of the 2001 IPELS Workshop*, Japan.
6. M. A. Shay and J. F. Drake, Geophys. Res. Lett. **25**, 3759 (1998).
7. J. Birn, J. F. Drake, M. A. Shay, et al., J. Geophys. Res.: Space. **106**, 3715 (2001).
8. R. G. Kleva, J. F. Drake, and F. L. Waelbroeck, Phys. Plasmas **2**, 23 (1995).
9. J. A. Breslau and S. C. Jardin, Comp. Phys. Communications, in press.
10. S. I. Braginskii, in *Reviews of Plasma Physics* (Consultants Bureau, New York, 1965), Vol. 1, p. 205.
11. J. B. Taylor, Phys. Rev. Lett. **33**, 1139 (1974).
12. W. Park, D. A. Monticello, and R. B. White, Phys. Fluids **27**, 137 (1984).
13. D. A. Uzdensky and R. M. Kulsrud, Phys. Plasmas **7**, 4018 (2000).
14. D. Biskamp and H. Welter, Phys. Rev. Lett. **44**, 1069 (1980).
15. L. C. Lee and Z. F. Fu, J. Geophys. Res. **91**, 6807 (1986).
16. J. Aparicio, et. al., Phys. Plasmas **5**, 3180 (1998).
17. H. E. Petschek, in *AAS-NASA Symposium on the Physics of Solar Flares*, NASA Special Publication **Sp-50**, 425 (1964).
18. D. Biskamp, E. Schwarz, and J.F. Drake, Phys. Plasmas **4**, 1002 (1997).
19. T. A. Carter, PhD Dissertation, Princeton University (2001).
20. D. Biskamp, et. al., Phys. Rev. Lett. **75**, 3850 (1995).

External Distribution

Plasma Research Laboratory, Australian National University, Australia
Professor I.R. Jones, Flinders University, Australia
Professor João Canalle, Instituto de Fisica DEQ/IF - UERJ, Brazil
Mr. Gerson O. Ludwig, Instituto Nacional de Pesquisas, Brazil
Dr. P.H. Sakanaka, Instituto Fisica, Brazil
The Librarian, Culham Laboratory, England
Library, R61, Rutherford Appleton Laboratory, England
Mrs. S.A. Hutchinson, JET Library, England
Professor M.N. Bussac, Ecole Polytechnique, France
Librarian, Max-Planck-Institut für Plasmaphysik, Germany
Jolan Moldvai, Reports Library, MTA KFKI-ATKI, Hungary
Dr. P. Kaw, Institute for Plasma Research, India
Ms. P.J. Pathak, Librarian, Insitute for Plasma Research, India
Ms. Clelia De Palo, Associazione EURATOM-ENEA, Italy
Dr. G. Grosso, Instituto di Fisica del Plasma, Italy
Librarian, Naka Fusion Research Establishment, JAERI, Japan
Library, Plasma Physics Laboratory, Kyoto University, Japan
Research Information Center, National Institute for Fusion Science, Japan
Dr. O. Mitarai, Kyushu Tokai University, Japan
Library, Academia Sinica, Institute of Plasma Physics, People's Republic of China
Shih-Tung Tsai, Institute of Physics, Chinese Academy of Sciences, People's Republic of China
Dr. S. Mirnov, TRINITI, Troitsk, Russian Federation, Russia
Dr. V.S. Strelkov, Kurchatov Institute, Russian Federation, Russia
Professor Peter Lukac, Katedra Fyziky Plazmy MFF UK, Mlynska dolina F-2, Komenskeho Univerzita, SK-842 15 Bratislava, Slovakia
Dr. G.S. Lee, Korea Basic Science Institute, South Korea
Mr. Dennis Bruggink, Fusion Library, University of Wisconsin, USA
Institute for Plasma Research, University of Maryland, USA
Librarian, Fusion Energy Division, Oak Ridge National Laboratory, USA
Librarian, Institute of Fusion Studies, University of Texas, USA
Librarian, Magnetic Fusion Program, Lawrence Livermore National Laboratory, USA
Library, General Atomics, USA
Plasma Physics Group, Fusion Energy Research Program, University of California at San Diego, USA
Plasma Physics Library, Columbia University, USA
Alkesh Punjabi, Center for Fusion Research and Training, Hampton University, USA
Dr. W.M. Stacey, Fusion Research Center, Georgia Institute of Technology, USA
Dr. John Willis, U.S. Department of Energy, Office of Fusion Energy Sciences, USA
Mr. Paul H. Wright, Indianapolis, Indiana, USA

The Princeton Plasma Physics Laboratory is operated
by Princeton University under contract
with the U.S. Department of Energy.

Information Services
Princeton Plasma Physics Laboratory
P.O. Box 451
Princeton, NJ 08543

Phone: 609-243-2750
Fax: 609-243-2751
e-mail: pppl_info@pppl.gov
Internet Address: http://www.pppl.gov